

This work has been submitted to the I3DA 2021 International Conference for possible publication in the IEEE Xplore Digital Library.

Copyright may be transferred without notice, after which this version may no longer be accessible.

Adding air attenuation to simulated room impulse responses: A modal approach

Brian Hamilton
Acoustics & Audio Group
University of Edinburgh
Edinburgh, UK
bhamilton.ac@gmail.com

Abstract—Air absorption is an important effect to consider when simulating room acoustics as it leads to significant attenuation in high frequencies. In this study, an offline method for adding air absorption to simulated room impulse responses is devised. The proposed method is based on a modal scheme for a system of one-dimensional dissipative wave equations, which can be used to post-process a room impulse response simulated without air absorption, thereby incorporating missing frequency-dependent distance-based air attenuation. Numerical examples are presented to evaluate the proposed method, along with comparisons to existing filter-based methods.

Index Terms—room acoustics, auralization, air absorption, modal methods

I. INTRODUCTION

Air absorption is an important source of attenuation in room acoustics and its emulation is critical to achieving realistic room acoustic simulations [1]. In general, air attenuation is a frequency-dependent and distance-based effect caused by viscothermal effects and relaxation processes [2]. While these physical processes may be modelled directly with wave-based models [3]–[5], the effect of air absorption is typically modelled with a set of digital filters [6]–[12]. Filter approaches have the potential to accurately reproduce air attenuation, but a common underlying problem is that filters must be tuned to accurately apply air attenuation. This comes with a trade-off between simplicity and accuracy – ranging from, e.g., octave-band approaches [13] to optimised IIR filters [12] and window-method FIR filters [11].

Recently, a more physically-motivated filtering approach was proposed [14], which is based on an approximate Green’s function to the viscothermal wave equation and side-steps many of the issues of pre-existing filter approaches. However, that approximate Green’s function approach is best suited to controlled indoor air conditions where power-law attenuation is sufficient for audible frequencies. The aim of this paper is to present a more general method that allows for post-processing a pre-computed room impulse response (RIR) with a complete air attenuation profile (i.e., classical power-law absorption plus two relaxation effects [2], [15], [16]) that can be used for all air conditions (temperature and humidity). This is particularly important when simulating partly-outdoor spaces, such as, e.g., medieval cathedrals [17] or other heritage/historic sites [18]–[21].

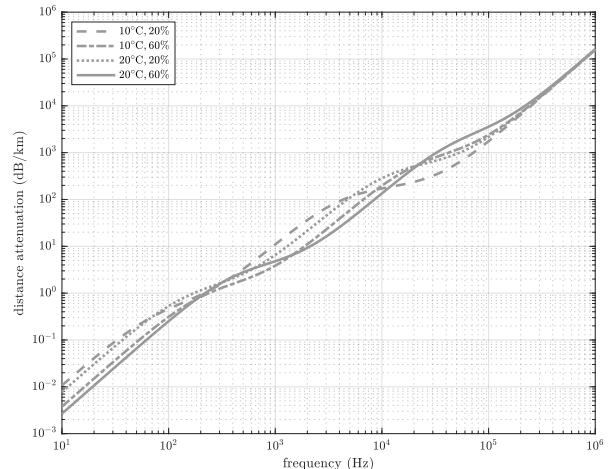


Fig. 1: Distance attenuation in dB/km as a function of frequency, for varying air conditions (temperature in degrees Celsius and relative humidity in percent).

The general aim of the proposed method is to use an input signal to drive a set of exponentially-damped plane waves, which travel a given distance such that the resulting output can be seen as frequency- and distance-based air attenuation having been applied to the input signal. As will be seen, this can be achieved with a system of dissipative wave equations which can be solved accurately and efficiently by a modal time-stepping scheme.

This paper is structured as follows. Section II presents background theory for air absorption and lossy wave propagation. Section III gives numerical schemes for lossy wave propagation, building towards a modal scheme of interest, along with numerical evaluations. Section IV presents the frequency-dependent modal scheme and procedure for adding air absorption to RIRs, along with numerical experiments testing its performance against a reference solution. Conclusions and final remarks are given in Section V.

II. BACKGROUND

A. Air absorption

Air absorption can be seen as a frequency-dependent distance-based damping on plane waves, written as:

$$p(t, x) = \hat{p}e^{-\alpha(\omega)x}e^{i(kx - \omega t)} \quad (1)$$

where p is a pressure, with a complex amplitude \hat{p} , real wavenumber k , real angular frequency ω , time t , and position x . $\alpha(\omega)$ is a frequency-dependent attenuation coefficient in Nepers/m which represents air absorption. Formulae for $\alpha(\omega)$ as a function of air temperature and humidity are left out for brevity but may be found in [15], [16]. See Fig. 1 for typical behaviour. For the purpose of this study it is sufficient to characterise this absorption by the property that $\alpha(\omega) \ll \omega/c$, such that $k \approx \omega/c$, where c is the speed of sound in air, which also means that the phase velocity can be assumed constant and equal to c .

B. Dissipative wave equation

In order to build up a physical system to achieve the desired result, we start by considering the one-dimensional lossy wave equation:

$$\partial_t^2 p + 2\sigma \partial_t p - c^2 \partial_x^2 p = 0 \quad (2)$$

where $p = p(t, x)$ is our wave-variable of interest (e.g., a pressure quantity), ∂_t^2 and ∂_x^2 denote second-order partial derivatives with respect to time and space, respectively, and σ is a loss constant in s^{-1} . A dispersion relation can be derived by considering a trial solution of the form:

$$p(t, x) = \hat{p} e^{i(kx - \omega t)} = \hat{p} e^{-\alpha x} e^{i(kx - \omega t)} \quad (3)$$

with complex wavenumber $\hat{k} = k + i\alpha$, where α is a constant (i.e., so far dissipation is not frequency-dependent). By insertion into (2) we get:

$$\hat{k}^2 = \frac{\omega^2}{c^2} + \frac{2i\sigma\omega}{c^2} \Rightarrow \hat{k} = \frac{\omega}{c} \sqrt{1 + \frac{2i\sigma}{\omega}} \quad (4)$$

We assume $\sigma \ll \omega$, for which we get $k \approx \omega/c$ and the approximate square root:

$$\hat{k} \approx \frac{\omega}{c} + i \frac{\sigma}{c} \quad (5)$$

Equating this to $\hat{k} = k + i\alpha$ we recover $\alpha \approx \sigma/c$.

It will be useful to set a boundary condition for this dissipative wave system that induces one-way travelling (plane-)wave solutions. One manner this can be achieved is through a forced boundary condition [22].¹

Returning to the time-space domain, let us consider this system on the domain $x \in [0, +\infty)$. At the left boundary we impose the condition:

$$p(t, 0) = u(t) \quad (6)$$

where $u(t)$ is some input signal used to drive the signal (with, otherwise, zero initial conditions for $x > 0$).

In the lossless case, $\sigma = 0$, it is straightforward to check that this boundary condition results in a rightward-travelling wave solution:

$$p(t, x) = u(t - x/c) \quad (7)$$

¹One-way wave equations exist and could also be used (e.g., convection-diffusion equations [23]). Second-order (two-way) wave equations are preferred here for favourable properties of associated numerical schemes.

When $\sigma > 0$, the system is dispersive and travelling-wave solutions – analogous to (7) – are not available. However, in the case of a time-harmonic $u(t) = \hat{u} e^{-j\omega t}$, it is straightforward to see that the solution on the domain $x \in [0, \infty)$ takes the form:

$$p(t, x) = \hat{u} e^{i(\hat{k}x - \omega t)} \quad (8)$$

with \hat{k} given by (4).

Let us then assume $u(t)$ can be written as the following sum of time-harmonic signals $u_q(t)$:

$$u(t) = \sum_{q=0}^{Q-1} u_q(t), \quad u_q(t) = \hat{u}_q e^{-i\omega_q t} \quad (9)$$

where ω_q are distinct (real) angular frequencies. Clearly, each component $u_q(t)$ would have the associated pressure solution $p_q(t, x) = \hat{p}_q e^{-\alpha x} e^{i(k_q x - \omega_q t)}$, and by linearity we have the solution:

$$p(t, x) = \sum_{q=0}^{Q-1} p_q(t, x) = \sum_{q=0}^{Q-1} \hat{u}_q e^{-\alpha x} e^{i(k_q x - \omega_q t)} \quad (10)$$

Thus, the general solution to this system, for $x \in [0, \infty)$, may be seen as a Fourier decomposition of damped, travelling plane waves, driven by the input signal $u(t)$.

III. NUMERICAL SCHEMES FOR LOSSY WAVE EQUATION

In this section we consider numerical schemes to simulate this lossy wave equation system. Consider a grid function $p_l^n \approx p(nT, (l + 1/2)X)$ with grid spacing X and time-step T , chosen to be $T = X/c$. Furthermore let $u^n = u((n - 1/2)T)$. In terms of these discrete functions, the lossless travelling wave solution (7) would translate to:

$$p_l^n = u^{n-l} \quad (11)$$

A. FDTD schemes

Although the intention is to derive and use a modal scheme, it will be informative to first discuss a simple FDTD scheme. The simplest finite-difference time-domain (FDTD) scheme in this setting [24] would be:

$$p_l^{n+1} = \frac{1}{1 + \sigma T} (p_{l+1}^n + p_{l-1}^n + (\sigma T - 1)p_l^{n-1}) \quad (12)$$

This scheme is known to be stable for $\sigma \geq 0$ [24]. To implement the boundary condition applied at $l = 0$, we can simply force the value at $l = 0$:

$$p_0^{n+1} = u^{n+1} \quad (13)$$

The above can be seen as a “hard source” – as opposed to a “soft source”, which would be a forcing term that additive to a pressure update [25], [26].

In the lossless case ($\sigma = 0$), this scheme permits the solution (11) and is thus *exact* (this can be verified by hand). This implies the scheme (12) is stable in the lossless case. It is expected that with the inclusion of the loss term $2\sigma \partial_t p$ – discretised here using the trapezoidal rule – stable is maintained under (13), although a stability analysis with the “hard source” boundary is not immediately available.

A close alternative boundary condition featuring a “soft source” is also available as:

$$p_0^{n+1} = \frac{1}{1 + \sigma T} (p_1^n + p_0^n + (\sigma T - 1)p_0^{n-1}) + F^n \quad (14)$$

where the “soft source” forcing term is denoted F^n :

$$F^n = \frac{1 + \sigma T/2}{1 + \sigma T} u^{n+1} - \frac{1 - \sigma T/2}{1 + \sigma T} u^n \quad (15)$$

The derivation for this update appears in the Appendix. It is straightforward to check that this scheme is also exact in the lossless case. Furthermore, a discrete energy balance may be obtained for this scheme (with $\sigma \geq 0$), from which stability can be proven (this is left out for brevity). In the presence of loss ($\sigma > 0$) these schemes are no longer exact, but they remain consistent with their underlying models.²

B. Semi-discrete modal schemes

With the target of simulating the general case of frequency-dependent dissipation, it will be convenient to consider modal schemes. To start we consider a semi-discrete modal scheme for this dissipative wave problem. For this we take the view that the solution is composed of modes (as per (10)) of the form:

$$p_q(t, x) = P_q(t) \cos(k_q x) \quad (16)$$

with $P_q(t)$ unknown. Inserting this trial solution into our PDE gives:

$$\ddot{P}_q(t) + 2\sigma \dot{P}_q(t) - c^2 k_q^2 P_q(t) = 0 \quad (17)$$

This ODE system ($q = 0, \dots, Q - 1$) can be solved with leapfrog integration, on a temporal-grid function $P_q^n \approx P_q(nT)$, or it can be solved with an “exact” recursion for the damped harmonic oscillator [24], [27], [28]:

$$P_q^{n+1} = 2e^{-\sigma T} \cos(\omega_q T) P_q^n - e^{-2\sigma T} P_q^{n-1} \quad (18)$$

where $\omega_q = \sqrt{c^2 k_q^2 + \sigma^2}$. This recursion is “exact” for solutions of the form $P_q^n = \hat{p}_q e^{-j\hat{\omega}_q nT}$, which can be verified by insertion into the above. In this semi-discrete time-space domain, the numerical solution would then be:

$$p(nT, x) = \sum_{q=0}^{Q-1} P_q^n \cos(k_q x) \quad (19)$$

C. Fully-discrete modal schemes

At this point we consider a fully-discrete modal scheme for our wave problem. For practical purposes we must truncate the domain of interest to some length L_x , such that $x \in [0, L_x]$. For our purposes, it is sufficient to assume $L_x = cT_d$ where T_d is a simulation duration of interest (this will be set to the duration of our pre-simulated input room impulse response). We consider a grid function $p_l^n \approx p(nT, (l + 1/2)X)$, with

$l = 0, \dots, N_x - 1$, with $N_x = \lceil L_x/X \rceil$, and $T = X/c$. For the modes, we choose the orthonormal cosine basis:

$$\Phi_{q,l} = a_q \cos\left(\frac{q\pi(l + 1/2)}{N_x}\right) \quad (20)$$

where $a_0 = \sqrt{\frac{1}{N_x}}$ and $a_q = \sqrt{\frac{2}{N_x}}$ for $q > 0$. As such, the solution is now assumed to take the form:

$$p_l^n = \sum_{q=0}^{Q-1} P_q^n \Phi_{q,l} \quad (21)$$

with $Q = N_x$.

It is insightful to write the full solution in matrix form. Let us define:

$$\mathbf{p}^n = [p_0^n, p_1^n, \dots, p_{N_x-1}^n]^T \quad (22a)$$

$$\mathbf{P}^n = [P_0^n, P_1^n, \dots, P_{Q-1}^n]^T \quad (22b)$$

$$\Phi_q = [\Phi_{q,0}, \Phi_{q,1}, \dots, \Phi_{q,N_x-1}]^T \quad (22c)$$

$$\mathbf{V} = [\Phi_0 | \Phi_1 | \dots | \Phi_{Q-1}] \quad (22d)$$

where \mathbf{V} is a $N_x \times N_x$ matrix, and \mathbf{p}^n , \mathbf{P}^n and Φ_q are $N_x \times 1$ vectors (and “ T ” denotes transposition), with $Q = N_x$. With these we have the ability to transform between time-space and modal domains via the matrix-vector products:

$$\mathbf{P}^n = \mathbf{V}^T \mathbf{p}^n, \quad \mathbf{p}^n = \mathbf{V} \mathbf{P}^n \quad (23)$$

and we note that $\mathbf{V} \mathbf{V}^T = \mathbf{I}$, where \mathbf{I} is an identity matrix. These matrix-vector products represent the Discrete Cosine Transform (DCT-II) and its inverse [29], respectively, which can be computed efficiently using a FFT-based algorithm [30].

The fully-discrete analogue to the modal update (18) is now:

$$\mathbf{P}^{n+1} = \mathbf{A} \circ \mathbf{P}^n - \mathbf{B} \circ \mathbf{P}^{n-1} \quad (24)$$

where “ \circ ” denotes an element-wise product, and

$$\mathbf{A} = 2 [e^{-\sigma T} \cos(\omega_0 T), \dots, e^{-\sigma T} \cos(\omega_{Q-1} T)]^T \quad (25a)$$

$$\mathbf{B} = [e^{-2\sigma T}, \dots, e^{-2\sigma T}]^T \quad (25b)$$

Next we consider the boundary condition (6), which we would like to implement in a “hard” manner analogous to (13). In order to derive this, let us introduce an intermediate grid function \tilde{p}_l^n , for which $\tilde{p}_l^n = p_l^n$ only when $l > 0$. Let us also define:

$$\tilde{\mathbf{p}}^n = [\tilde{p}_0^n, \tilde{p}_1^n, \dots, \tilde{p}_{N_x-1}^n]^T \quad (26a)$$

$$\tilde{\mathbf{P}}^n = \mathbf{V}^T \tilde{\mathbf{p}}^n \quad (26b)$$

$$\delta = [1, 0, \dots, 0]^T \quad (26c)$$

i.e., $\tilde{\mathbf{p}}^n$ is the vector form of \tilde{p}_l^n and $\tilde{\mathbf{P}}^n$ its modal form, and δ is a Kronecker delta in vector form.

We would like to express p_l^{n+1} as \tilde{p}_l^{n+1} plus a correction, such that (13) is satisfied. Clearly, this would be as simple as setting:

$$p_0^{n+1} = \tilde{p}_0^{n+1} + (u^{n+1} - \tilde{p}_0^{n+1}) \quad (27)$$

This could also be written as:

$$\mathbf{p}^{n+1} = \tilde{\mathbf{p}}^{n+1} + \delta(u^{n+1} - \delta^T \tilde{\mathbf{p}}^{n+1}) \quad (28)$$

²This is primarily due to the fact that the introduction of loss in (12) upsets a delicate balance of approximation errors in space and time from the lossless case [24].

Left-multiplying by \mathbf{V}^T , we have in the modal domain:

$$\mathbf{P}^{n+1} = \tilde{\mathbf{P}}^{n+1} + \mathbf{V}^T \delta \left(u^{n+1} - \delta^T \mathbf{V} \tilde{\mathbf{P}}^{n+1} \right) \quad (29)$$

Let us now define:

$$\phi = \mathbf{V}^T \delta = [\Phi_{0,0}, \Phi_{1,0}, \dots, \Phi_{Q-1,0}]^T \quad (30)$$

We can then propose the following scheme update with a “hard source” correction (forced-boundary):

$$\tilde{\mathbf{P}}^{n+1} = \mathbf{A} \circ \mathbf{P}^n - \mathbf{B} \circ \mathbf{P}^{n-1} \quad (31a)$$

$$\mathbf{P}^{n+1} = \tilde{\mathbf{P}}^{n+1} + \phi \left(u^{n+1} - \phi^T \tilde{\mathbf{P}}^{n+1} \right) \quad (31b)$$

This update is exact for the lossless case since it is, in fact, the exact FDTD scheme ((12) and (13) via (27)) transformed to a modal update.³ It is not expected to be exact in the presence of loss since the hard boundary is applied at $x = X/2$ and not $x = 0$, which means there is a small distance over which dissipation is not incurred (this error is negligible for practical purposes).

Alternatively, one can apply a simpler “soft source” update, for which the modal update becomes:

$$\mathbf{P}^{n+1} = \mathbf{A} \circ \mathbf{P}^n - \mathbf{B} \circ \mathbf{P}^{n-1} + F^n \phi \quad (32)$$

where F^n is the forcing term (15).⁴ This update is also exact in the lossless case, but it is expected to be less accurate than (31) when $\sigma > 0$. However, this update has the advantage that stability is straightforward to establish through Z-transform analysis.

D. Validation of frequency-independent dissipative schemes

A simple test is conducted to evaluate the numerical schemes presented thus far. The case of zero loss will not be tested (for brevity) since exactness may be verified by hand. As for the lossy case $\sigma > 0$, Fig. 2 displays simulated one-way dissipative wave propagation with a raised-cosine input signal $u(t)$ with dissipation set for a 60dB decay time of $6 \ln(10) \sigma^{-1} = 1.0$ s. Displayed in the figure are $p(t, x)$ simulated using the FDTD schemes with “hard” and “soft” boundary updates, as well as using the corresponding modal schemes. It can be seen that the four simulations display similar behaviour, but differences are apparent in the wake of the travelling wave (see zoom overlay in Fig. 2c). For example, the “soft-FDTD” does not satisfy the boundary condition with the chosen raised-cosine input (one can note a slight DC offset at $x = 0$), whereas the “hard-FDTD” output displays a slope in the wake of the wave which is absent from modal outputs. In regards to the “soft”

³This will be not be shown, but the proof is carried out using the known eigenvalues/eigenvectors of the corresponding Laplacian matrix (see, e.g., [29]) or by Taylor series expansion (see, e.g., [31]).

⁴It may be noted that (32) is similar to the modal time-stepping update presented in [28] – particular in the choices of time-stepping update and of a cosine modal basis. The numerical modal method in [28], paired with domain decomposition, was ultimately used for 3-D wave simulations with damping that similarly mimics air attenuation. However, the scheme here is limited to one spatial dimension, and the “soft” forcing term given here is of a different nature than that in [28] – derived here specifically to satisfy the boundary condition (6).

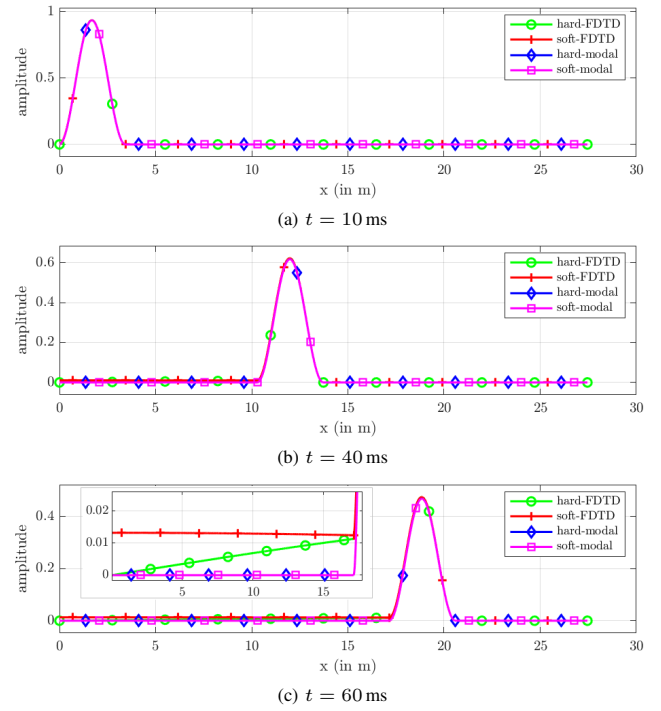


Fig. 2: Examples of simulated one-way dissipative wave propagation at different time instances t , using raised cosine input $u(t)$ with 60dB decay time $6 \ln(10) \sigma^{-1} = 1.0$ s and speed of sound $c = 343$ m/s. All schemes using time-step $T = (48 \text{ kHz})^{-1}$. The last image displays an overlay to show detail in wake behaviour.

updates, it should be noted that in this case the assumption $\sigma \ll \omega$ is not satisfied for low frequencies.

For the remainder of this paper we will consider only modal methods, but it is worth mentioning that what follows could be achieved with FDTD methods using a more general – and indeed more “physically valid” – second-order wave equation with air absorption processes included (after [5]). However, in that case we would be faced with numerical dissipation errors – even with a domain limited to one spatial dimension⁵ – and this would necessitate grid refinement; whereas the “exact” modal schemes are essentially free from dissipation errors (and are, accordingly, more efficient for this specific application).

IV. MODAL SCHEME FOR SIMULATING AIR ABSORPTION

In this section we extend the modal scheme to the frequency-dependent case to incorporate air attenuation. Since each mode in the system is independent the modal damping coefficients can be set individually for each mode (as in, e.g., [28], [37]).

⁵Numerical phase velocity errors will be minimal in such 1-D FDTD schemes (and non-existent in the lossless case [32], [33]), but numerical dissipation errors may be significant in high frequencies when discretising loss terms using conventional means (trapezoid rule) – e.g., as reported in [5], [34] with regards to the problem of air absorption. Without resorting to higher-accurate schemes (with less favourable stability properties), such dissipation errors can only be overcome with oversampling, which would increase computational costs. An analogous issue has been reported in the context of FDTD modelling of musical strings [35], where a possible solution is to optimise parameters for fictitious loss terms in the discrete domain to minimize numerical dissipation errors [36].

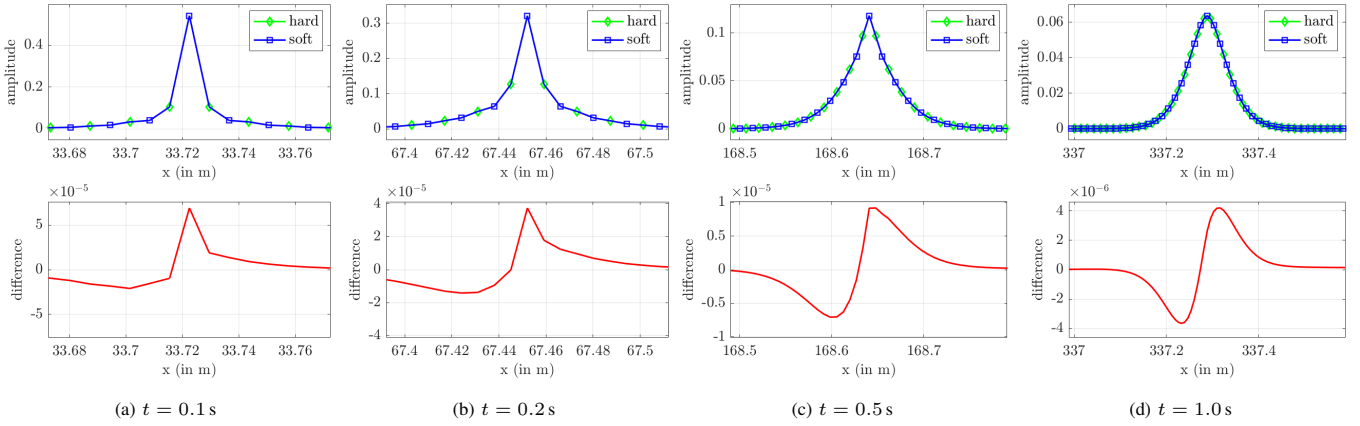


Fig. 3: Examples of simulated one-way dissipative wave propagation with modal schemes using “soft” and “hard” boundary conditions (and differences), at different time instances t , using Kronecker delta input ($u^n = [1, 0, \dots, 0]$) with decay constants σ_q set from air attenuation model for air temperature 10°C and 20% relative humidity ($c = 337 \text{ m/s}$). Modal time-stepping using time-step $T = (48 \text{ kHz})^{-1}$.

It suffices then to replace σ by $\sigma_q = c\alpha(\omega_q)$. Note that with realistic air absorption (see, e.g., Fig. 1), it can be assumed that $\alpha(\omega) \ll \omega/c$ for all frequencies of interest (audible frequencies).

In terms of a PDE system, we have then Q lossy wave equations ($q = 0, \dots, Q-1$), each with its own damping coefficient:

$$\partial_t^2 p_q + 2\sigma_q \partial_t p_q - c^2 \partial_x^2 p_q = 0 \quad (33a)$$

$$p_q(t, 0) = u_q(t) \quad (33b)$$

We take the associated solution:

$$p(t, x) = \sum_{q=0}^{Q-1} p_q(t, x) = \sum_{q=0}^{Q-1} \hat{u}_q e^{-\alpha_q x} e^{i(k_q x - \omega_q t)} \quad (34)$$

where $ck_q = \sqrt{\omega_q^2 + \sigma_q^2}$, and where $u(t)$ is related to $\hat{u}_q e^{-i\omega_q t}$ through (9).

Our fully-discrete modal scheme with “hard” boundary keeps the form (31), but now with

$$\mathbf{A} = [2e^{-\sigma_0 T} \cos(\omega_0 T), \dots, 2e^{-\sigma_{Q-1} T} \cos(\omega_{Q-1} T)]^T \quad (35a)$$

$$\mathbf{B} = [e^{-2\sigma_0 T}, \dots, e^{-2\sigma_{Q-1} T}]^T \quad (35b)$$

Meanwhile, the modal scheme with the “soft source” boundary now takes the form:

$$\mathbf{P}^{n+1} = \mathbf{A} \circ \mathbf{P}^n - \mathbf{B} \circ \mathbf{P}^{n-1} + \mathbf{F}^n \circ \phi \quad (36)$$

with \mathbf{A} and \mathbf{B} changed as noted previously, and the forcing term taking the *vector* form:

$$\mathbf{F}^n = [F_0^n, F_1^n, \dots, F_{Q-1}^n]^T \quad (37a)$$

$$F_q^n = \frac{1 + \sigma_q T/2}{1 + \sigma_q T} u^{n+1} - \frac{1 - \sigma_q T/2}{1 + \sigma_q T} u^n \quad (37b)$$

A. Validation of modal schemes and comparisons with filter methods

Numerical tests are presented in order to compare and validate the frequency-dependent modal schemes in the context of air absorption. For the following tests, air conditions of 10°C temperature and 20% relative humidity are chosen so that air absorption deviates significantly from classical power-law attenuation in the audible frequencies (see Fig. 1).

Fig. 3 shows simulated one-way dissipative wave propagation with a Kronecker delta input with dissipation set to mimic the desired air attenuation. Displayed in the figure are $p(t, x)$ simulated using the modal schemes with “hard” and “soft” boundary update, and differences between them. It can be seen that the schemes return similar results with small differences.

To validate the modal schemes in their reproduction of a target air attenuation, we can simply measure the attenuation at a given time instant (corresponding to a distance travelled) and compare to the “analytic” air absorption model (from [15]). For the same conditions above, Fig. 4a shows the attenuation per distance (in km) simulated, calculated at time instant $t = 1.0 \text{ s}$, along with the target air attenuation curve. It can be seen that agreement with the target air attenuation is excellent (as expected for these modal schemes). Results are identical for other time instances and are thus left out for brevity.⁶

In contrast, a more conventional filter approach is plotted in Fig. 4b, in which third-order Butterworth octave-band filters are used as a analysis/synthesis filter bank used to process a 48 kHz-sample-rate Kronecker delta input with distance-based exponential damping applied to mimic air absorption (sampled at 11 octave-band centre frequencies) – as may be found in traditional geometrical acoustics room simulations such as, e.g., [13]. Ripples are apparent in the attenuation simulated by the filterbank approach, as one might expect. This can be improved using a filterbank of 1/3-octave band filters (as in,

⁶However, for very large distances dissipation can be sufficient to exceed the relative accuracy of finite-precision, and – only in those cases – simulated measurements of air attenuation will not return accurate results.

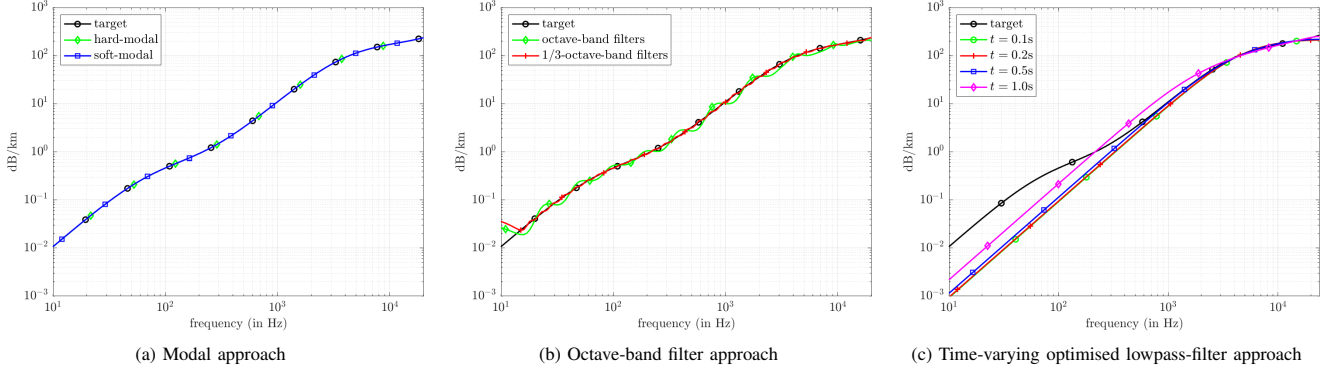


Fig. 4: Simulated air attenuation using modal schemes and digital-filter approaches, and target air attenuation for air temperature 10°C and 20% relative humidity ($c = 337$ m/s). Modal time-stepping using time-step $T = (48 \text{ kHz})^{-1}$. Filter methods use 48 kHz sample rates. Octave-band filters are of third-order Butterworth type, and optimised lowpass-filter approach is using the method presented in [12].

e.g., [10]), which, if chosen well, leads to more tightly-fitting ripples, as seen in the same figure (here, using 32 1/3-octave-band filters of third-order Butterworth type). Another potential option would be the use of FIR partition-of-unity filters [38].

Additionally, results from an alternative, recently-presented [12], optimised IIR filter approach is plotted in Fig. 4c. This method is based on a set of triple-cascaded first-order lowpass filters optimised for attenuation tuned to distances corresponding to each sampling instant [12]. A Kronecker delta is filtered to measure simulated attenuation tuned to different time instants (distances). In the figure it can be seen that this approach does well to reproduce attenuation in high frequencies (where it is most significant), but errors appear in low frequencies. On the other hand, one can note that simulated attenuation curves vary as a function of time instant, and for longer times (higher attenuation) attenuation filters deviate more from the target attenuation (in dB/km).⁷

B. Adding air absorption to simulated RIRs

It remains to detail the procedure to add air absorption to a pre-simulated RIR (simulated without air absorption) using the presented modal schemes. Consider then a finite-duration discrete RIR signal $h[n]$ with sample rate $1/T$ (e.g., 48 kHz), with N_t samples, indexed by $n' = 0, \dots, N_t - 1$. Of course, $h[n]$ can be seen as a linear combination of N_t shifted and scaled Kronecker deltas. We have shown that the distance-based attenuation is accurately reproduced for a Kronecker delta input, so it follows that we can simply apply the same procedure to the signal itself to process each individual sample. Since the system is linear and time-invariant, all such samples can be processed simultaneously (i.e. in a single modal simulation).

We must ensure that correct distance attenuation is applied to each sample n , where that distance would be simply $d = c(n + 1/2)T$ (in m).⁸ For this we must *time-reverse* the input RIR

⁷To produce data for the optimised lowpass filter approach [12], Matlab code provided as supplementary material to [12] was used, but reconfigured to optimise over 20 Hz–20 kHz with approximately 40k frequency samples.

⁸Here we assume a constant speed of sound c , but it is important in practice that any “pre-delay” in the signal be removed (or compensated for in the application of attenuation).

as we feed it into the system (via the left-boundary condition); i.e., we can set the forcing signal to our ODE system to be:

$$u^n = h[N_t - 1 - n] \quad (38)$$

We can then run the forced modal schemes with $Q = N_t$ modes for N_t time-steps, starting from zero initial conditions ($\mathbf{P}^{-1} = \mathbf{P}^{-2} = 0$). The output RIR with air attenuation added, which we will denote $h'[n]$, can then be read from the final state of our wave simulation as follows:

$$h'[n] = p_n^{N_t-1}, \quad n = 0, \dots, N_t - 1 \quad (39)$$

where $p_n^{N_t-1}$ are simply the elements of $\mathbf{p}^{N_t-1} = \mathbf{V}\mathbf{P}^{N_t-1}$. Note that the entire simulation can be run in the modal domain. Projection back to a spatial grid (with N_x points) is only needed at the end, and this can be accomplished using a fast inverse DCT-II algorithm [30].

When losses are disabled ($\sigma_q = 0$), the proposed procedure will simulate the solution (13) and return $h'[n] = h[n]$, as desired. Also, it is recommended that the “soft” update be used for the application of air absorption, since we have seen that “hard” and “soft” boundary updates give similar results, and the soft update ultimately requires fewer operations.

C. A reference solution

At this point it is useful to introduce a “reference solution” for the problem of adding air absorption to a RIR. Taking $h[n]$ and $h'[n]$ as a $N_t \times 1$ vectors:

$$\mathbf{h} = [h[0], h[1], \dots, h[N_t - 1]]^T \quad (40a)$$

$$\mathbf{h}' = [h'[0], h'[1], \dots, h'[N_t - 1]]^T \quad (40b)$$

We can propose a reference solution:

$$\mathbf{h}' = \mathbf{\Omega}\mathbf{V}^T\mathbf{h} \quad (41)$$

where $\mathbf{\Omega}$ is a $N_t \times N_t$ matrix with elements at rows q and columns l (with zero-based indexing) given by:

$$\Omega_{q,l} = e^{-\alpha_q x_l} \Phi_{q,l} \quad (42)$$

where $x_l = (l + 1/2)X$ and where $\Phi_{q,l}$ is given by (20). This reference solution is simply a decomposition of a signal onto

an orthonormal cosine basis and a subsequent projection back onto the same basis weighted by distance-based air attenuation, under the assumption that the l th sample travels x_l metres. This can ultimately be seen as a limiting case of the frequency-band filterbank approach, where here N_t frequency bands are used. Note that when $\alpha_q = 0$ (41), $\mathbf{\Omega} = \mathbf{V}$, and (41) returns $\mathbf{h}' = \mathbf{h}$ (as desired). However, this is not claimed to be an analytic solution to the dissipative wave problems seen before, nor to the more general second-order wave systems with air absorption processes [2], [5]; it should be seen as a “brute-force” application of air attenuation under the assumptions used in this study.

In terms of its compute cost, for $\alpha_q > 0$ this reference solution is somewhat impractical for the reason that N_t should be on the order of 10^4 – 10^5 , and only the matrix-vector product $\mathbf{y} = \mathbf{V}^T \mathbf{h}$ (DCT-II) can use a fast FFT-based algorithm [30]. The matrix-vector product $\mathbf{\Omega} \mathbf{y}$ must be computed directly, and this would require N_t^2 evaluations of transcendental functions, and N_t^2 storage (if $\mathbf{\Omega}$ is precomputed). More will be said about computational complexity later.

D. Numerical examples

In order to test the application of air absorption to a RIR using this modal scheme (with “soft” boundary update), we conduct a simple image source simulation [39]. A room of size $7.2 \times 5.1 \times 4.3$ (in m) is chosen with a Sabine-absorption coefficient of 0.045, with a source and receiver at positions (6.1, 2.0, 1.1) and (3.3, 3.1, 1.3) respectively. Image source distances are randomly perturbed by a relative amount in range $[-1\%, +1\%]$ in order to eliminate sweeping echoes due to perfect rectangular symmetry [40] (and ultimately increasing diffuseness in the room). Air conditions are as before (10°C and 20% relative humidity) with a corresponding speed of sound $c = 337$ m/s. A RIR, $h[n]$, is simulated at 48kHz, and its spectrogram – computed with 1024-sample Hann-windowing and 75% frame overlap – is displayed in Fig. 5a. Using $h[n]$ as input to the modal scheme (using the time-reversed procedure described previously) returns a modified RIR, $h'[n]$, whose spectrogram is displayed in Fig. 5b, where the effect of air absorption is clearly seen. The corresponding reference solution is shown in Fig. 5c. Additionally, air attenuation is added to $h[n]$ with the overlap-add (OLA) approach (STFT processing) (after [11], [41]) and shown in Fig. 5d.⁹ Agreements are excellent between the three methods, at least from the point of view of spectrograms.

For a more objective comparison, it is useful to compute similarities between STFT frames corresponding to the spectrograms in Fig. 5. This can be accomplished with the following geometric similarity index:

$$\chi[n] = \frac{\|Y_1(n, \omega) Y_2^*(n, \omega)\|_\omega}{\|Y_1(n, \omega)\|_\omega \|Y_2(n, \omega)\|_\omega} \quad (43)$$

⁹For OLA processing, a Hann window of length 1024 samples was used for analysis and synthesis windows, scaled for a constant unity overlap-add envelope (with sufficient zero padding to provide perfect reconstruction in lossless case), with air absorption applied to STFT frames by frequency-domain multiplication.

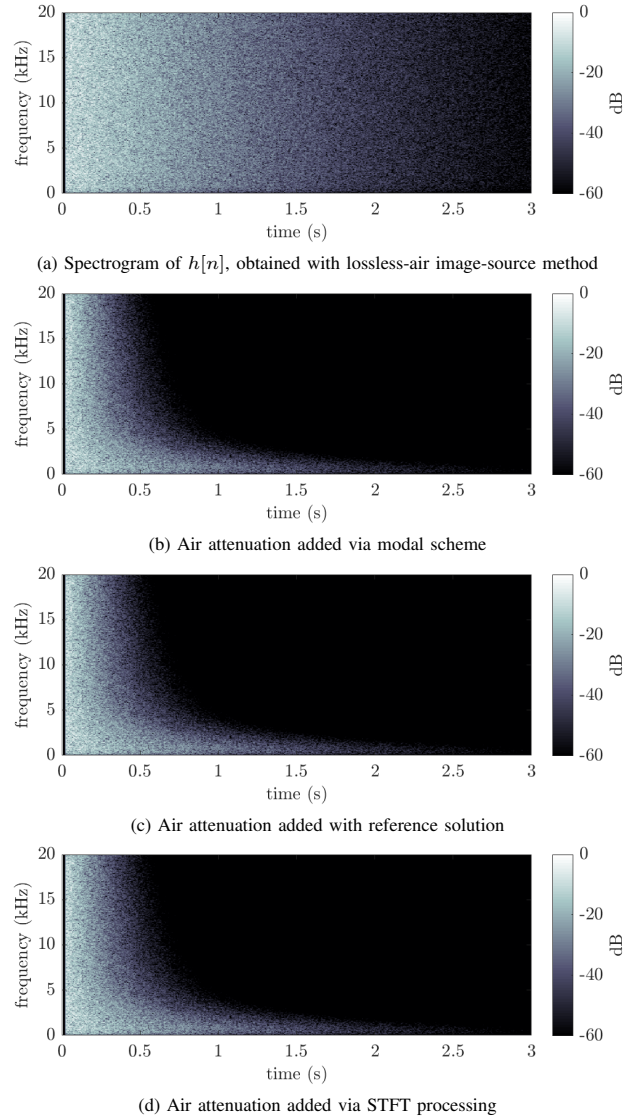


Fig. 5: Spectrograms of room impulse response, simulated with image source method, with and without air absorption added.

Here $Y_1(n, \omega)$ and $Y_2(n, \omega)$ represent the STFTs of two discrete-time signals $y_1[n]$ and $y_2[n]$, and the Euclidean norms are calculated across the frequency-dimension, and $0 \leq \chi[n] \leq 1$. Comparing to the reference solution, in Fig. 6 we plot $\log_{10}(1 - \chi)$ for the hard-modal output, and the output from the OLA method, along with the output of the soft-modal scheme (corresponding spectrogram not shown for brevity). It can be seen that the outputs generated are extremely similar to the reference solution, with modal schemes performing best, generally by an order of magnitude or more (in terms of frame similarity). Indeed, the OLA method, at least as implemented here, would seem to perform more than well enough for practical use. With that said, it should be remarked that this constitutes the first evaluation of the accuracy of the OLA approach in the literature (to the author’s knowledge).

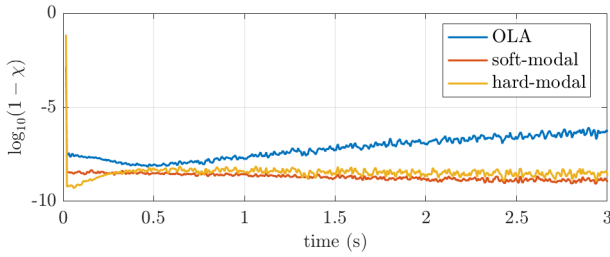


Fig. 6: RIR STFT frame similarities (43) to reference solution (see Fig. 5).

V. CONCLUSIONS AND FINAL REMARKS

A method to add general air absorption to simulated room impulse responses was provided in this paper. The method uses a fully-discrete modal scheme with boundary conditions chosen for one-way dissipative wave propagation, such that accurate frequency-dependent, distance-based air attenuation may be applied to an input RIR. FDTD schemes were used to help derive a “soft source” boundary update, which was also compared to a “hard” forced-boundary update. Frequency-dependent modal schemes were validated against target air attenuation curves, along with existing filter-based approaches. An image source room simulation was used to test the application of air attenuation to a RIR, and this was compared to air attenuation applied via STFT-based time-frequency processing.

The method presented is advantageous for its generality (it can apply air attenuation for any air conditions) and because it does not need tuning or optimisation as required in filter-based methods. On the other hand, this method is more computationally demanding than filter-based methods, which would be more applicable to real-time applications. This modal approach is better suited to offline data generation (as needed for, e.g., auditory research [42] or speech dereverberation [43]). Additionally, this approach is well-suited to complement (offline) RIR simulation with 3-D wave-based methods [44], [45], where modelling air absorption processes directly leads to significant increases in memory usage (e.g., at minimum 50% more memory than lossless wave-equation schemes [5], [34]).

With regards to computational costs, the complexity of the presented modal is $O(N_t^2)$ where N_t is the number of samples to be computed, which is similar to a 1-D FDTD scheme (in the lossy case [24]). On the other hand, time-frequency processing via STFT would be $O(\frac{N_t}{H} M \log_2 M)$ where M is the frame size (assumed power of two) and $1 \leq H \leq M$ is the hop size in samples. While it is possible for the OLA method to have higher complexity than the modal approach (depending on choices of M and H), in practice it is expected that the complexity should be lower for STFT-based processing (usually $M \ll N_t$). Low-order IIR filter-based approaches would usually be $O(N_t)$, but frequency-band approaches would reach $O(N_t^2)$ in the high-resolution limit of N_t frequency bands. The reference solution provided here can be seen as such a limiting filterbank – and is accordingly also $O(N_t^2)$ – but

should be less efficient than modal recursion because of the need for evaluation of N_t^2 exponentially-damped-cosine matrix elements.

In regards to compute times, it must also be noted that modal updates are highly, and easily, parallelisable (each mode can be updated in parallel), and processing a RIR with this modal approach could be accomplished in only a few seconds on a modern desktop computer (with an optimised multithreaded code – see, e.g., [37]), even with N_t on the order of 10^5 . To keep the number of modes ($Q = N_t$) to a minimum the sampling rate of the input RIR should be not be higher than necessary for audio purposes.

Finally, it should be mentioned that the presented approach is only applicable to static scenes (precluding moving sources or receivers), but allows for source/receiver directivity [46], [47]. It could also be used for outdoor scenes provided that wind is not significant. On the other hand, for typical indoor conditions (e.g., 20°C, 50% humidity), it may be sufficient to view air absorption as a simple power-law attenuation, in which case the Green’s function method recently presented in [14] may be preferable with its $O(N_t)$ complexity and applicability to real-time usage. In future work, the various methods of applying air attenuation to a simulated RIR could be compared on a perceptual basis (through listening tests).

ACKNOWLEDGMENT

Thanks to Michele Ducceschi, Charlotte Desvages, and James-Michael Leahy for fruitful discussions on topics relating to numerical modelling of dissipative wave propagation.

APPENDIX

A. Boundary condition for lossy wave equation

We consider a semi-infinite domain terminated at $x = 0$ (and extending towards $+\infty$) with PDE (2) and desired boundary condition (6).

An energy analysis reveals that one can set the left boundary as:

$$\partial_x p(t, x)|_{x=0} = -f(t) \quad (\text{A.1})$$

where $f(t)$ is an unspecified forcing signal to be associated to $u(t)$. Following [22], but here with dissipation included, one can impose a rightward-travelling plane-wave solution of the form:

$$p(t, x) = \hat{p} e^{i(\hat{k}x - \omega t)} \quad (\text{A.2})$$

where $\hat{k} = k + i\alpha$.

By linearity, we take $u(t) = \hat{u} e^{-i\omega t}$ and $f(t) = \hat{f} e^{-i\omega t}$. From (6) and (A.1), we get at the left boundary:

$$p(t, 0) = \hat{u} e^{-i\omega t} \quad (\text{A.3})$$

and

$$\partial_x p(t, x)|_{x=0} = i(k + i\alpha)u(t) \quad (\text{A.4})$$

which implies $f(t) = -i\hat{k}u(t)$. With $k \approx \omega/c$, we then have:

$$\partial_x p(t, x)|_{x=0} = -\frac{1}{c}(c\alpha - i\omega)u(t) \quad (\text{A.5})$$

and

$$\partial_x p(t, x)|_{x=0} = -\frac{1}{c}(\sigma u(t) + \dot{u}(t)) \quad (\text{A.6})$$

B. Soft-source FDTD boundary condition for lossy wave equation

We can discretise (A.6) at $l = 0$ with:

$$\frac{p_0^n - p_{-1}^n}{X} = -\frac{1}{c} \left(\sigma \frac{u^{n+1} + u^n}{2} + \frac{u^{n+1} - u^n}{T} \right) \quad (\text{A.7})$$

Solving for the ghost point p_{-1}^n with $T = X/c$, and inserting into (12) at $l = 0$, we get:

$$p_0^{n+1} = \frac{1}{1 + \sigma T} (p_1^n + p_0^n + (\sigma T - 1)p_0^{n-1}) + \underbrace{\frac{1 + \sigma T/2}{1 + \sigma T} u^{n+1} - \frac{1 - \sigma T/2}{1 + \sigma T} u^n}_{F^n} \quad (\text{A.8})$$

where the “soft source” forcing term is denoted F^n . It is straightforward to check by hand that (11) satisfies this update when $\sigma = 0$, and thus remains exact in the lossless case. Furthermore, in the lossless case, this can be seen as a consistent discretisation of:

$$\partial_t^2 p - c^2 \partial_x^2 p = c\delta(x - \varepsilon)\dot{u}(t) \quad (\text{A.9a})$$

$$\partial_x p|_{x=0} = 0 \quad (\text{A.9b})$$

in the limit of $\varepsilon \rightarrow 0$ ($\varepsilon \geq 0$). This is a system that has the identical one-way travelling wave solution (7), which can be verified through the known Green’s function to the lossless 1-D wave equation and the principle of mirror images (with two travelling waves coalescing in the limit of $\varepsilon \rightarrow 0$). By the same token, the lossy FDTD scheme can be seen as a discretisation of the following PDE system:

$$\partial_t^2 p + 2\sigma \partial_t p - c^2 \partial_x^2 p = c\delta(x - \varepsilon)(\sigma u(t) + \dot{u}(t)) \quad (\text{A.10a})$$

$$\partial_x p|_{x=0} = 0 \quad (\text{A.10b})$$

in the limiting case of $\varepsilon \rightarrow 0$. This would imply that the system consisting of (2) and (A.6) has the same solutions as (A.10), under the assumption that $\frac{1}{X}\delta[0]$, a scaled Kronecker delta, is a discretisation of $\delta(x - \varepsilon)$ in the limit of $\varepsilon \rightarrow 0$ on the chosen grid (where $l = 0$ pertains to $x = X/2$). As such, the forcing term F^n may also be used in the modal update (32), where the chosen cosine basis already satisfies the boundary condition (A.10b).

REFERENCES

- [1] M. Vorländer, *Auralization: Fundamentals of Acoustics, Modelling, Simulation, Algorithms and Acoustic Virtual Reality*, Springer, 2nd edition, 2020.
- [2] A. D. Pierce, *Acoustics*, chapter Effects of Viscosity and Other Dissipative Processes, Springer, 2019.
- [3] M. S. Wochner, A. A. Atchley, and V. W. Sparrow, “Numerical simulation of finite amplitude wave propagation in air using a realistic atmospheric absorption model,” *J. Acoust. Soc. Am.*, vol. 118, no. 5, pp. 2891–2898, 2005.
- [4] N. Jiménez, F. Camarena, J. Redondo, V. Sánchez-Morcillo, Y. Hou, and E. E. Konofagou, “Time-domain simulation of ultrasound propagation in a tissue-like medium based on the resolution of the nonlinear acoustic constitutive relations,” *Acta Acustica united with Acustica*, vol. 102, no. 5, pp. 876–892, 2016.
- [5] B. Hamilton and S. Bilbao, “FDTD modelling of sound propagation in air including viscothermal and relaxation effects,” in *Proc. e-Forum Acusticum*, Lyon, France, Dec. 2020.
- [6] J. A. Moorer, “About this reverberation business,” *Comp. Music J.*, pp. 13–28, 1979.
- [7] J.-M. Jot and A. Chaigne, “Digital delay networks for designing artificial reverberators,” in *AES Convention 90*. Audio Engineering Society, 1991.
- [8] J. Huopaniemi, L. Savioja, and M. Karjalainen, “Modeling of reflections and air absorption in acoustical spaces a digital filter design approach,” in *Proc. IEEE Worksh. Appl. Signal Process. Audio & Acoust.*, 1997, pp. 4–pp.
- [9] L. Savioja, T. Huopaniemi, J. and Lokki, and R. Väänänen, “Creating interactive virtual acoustic environments,” *J. Audio Eng. Soc.*, vol. 47, no. 9, pp. 675–705, Sept. 1999.
- [10] D. Schröder, *Physically based real-time auralization of interactive virtual environments*, vol. 11, Logos Verlag Berlin GmbH, 2011.
- [11] J. Saarelma, J. Califa, and R. Mehra, “Challenges of distributed real-time finite-difference time-domain room acoustic simulation for auralization,” in *AES Int. Conf. Spatial Reproduction*, July 2018.
- [12] J. M. Kates and E. J. Brandewie, “Adding air absorption to simulated room acoustic models,” *J. Acoust. Soc. Am.*, vol. 148, no. 5, pp. EL408–EL413, 2020.
- [13] R. Scheibler, E. Bezzam, and I. Dokmanić, “Pyroomacoustics: A Python package for audio room simulation and array processing algorithms,” in *Proc. IEEE Int. Conf. Acoust., Speech, Signal Process.*, 2018, pp. 351–355.
- [14] B. Hamilton, “Air absorption filtering method based on approximate Green’s function for Stokes’ equation,” in *Proc. Digital Audio Effects (DAFx)*, Vienna, Austria, Sept. 2021, (accepted for publication).
- [15] “Acoustics – Attenuation of sound during propagation outdoors. Part 1: Calculation of the absorption of sound by the atmosphere,” Standard ISO 9613–1, International Organization for Standardization, Geneva, Switzerland, 1993.
- [16] H. E. Bass, L. C. Sutherland, A. J. Zuckerwar, D. T. Blackstock, and D. M. Hester, “Atmospheric absorption of sound: Further developments,” *J. Acoust. Soc. Am.*, vol. 97, no. 1, pp. 680–683, 1995.
- [17] B. N. J. Postma and B. F. G. Katz, “Acoustics of Notre-Dame Cathedral de Paris,” in *Proc. Int. Symp. Music & Room Acoust.*, Buenos Aires, Argentina, Sept. 2016.
- [18] G. Iannace and A. Trematerra, “The acoustics of the caves,” *Appl. Acoust.*, vol. 86, pp. 42–46, 2014.
- [19] D. Murphy, S. Shelley, A. Foteinou, J. Brereton, and H. Daffern, “Acoustic heritage and audio creativity: The creative application of sound in the representation, understanding and experience of past environments,” *Internet Archaeology*, 2017.
- [20] B. F. G. Katz, D. Murphy, and A. Farina, “Exploring cultural heritage through acoustic digital reconstructions,” *Physics Today*, vol. 73, no. 12, pp. 32–37, 2020.
- [21] D. D’Orazio, G. Fratoni, E. Rossi, and M. Garai, “Understanding the acoustics of st. john’s baptistry in pisa through a virtual approach,” *J. Building Performance Simulation*, vol. 13, no. 3, pp. 320–333, 2020.
- [22] L. E. Kinsler, A. R. Frey, A. B. Coppens, and J. V. Sanders, *Fundamentals of Acoustics*, John Wiley & Sons, 4th edition, 2000.
- [23] J. Strikwerda, *Finite Difference Schemes and Partial Differential Equations*, SIAM, Philadelphia, PA, 2004.
- [24] S. Bilbao, *Numerical Sound Synthesis: Finite Difference Schemes and Simulation in Musical Acoustics*, Wiley, 2009.
- [25] J. Sheaffer, M. van Walstijn, and B. Fazenda, “Physical and numerical constraints in source modeling for finite difference simulation of room acoustics,” *J. Acoust. Soc. Am.*, vol. 135, no. 1, pp. 251–261, 2014.
- [26] J. Botts and L. Savioja, “Effects of sources on time-domain finite difference models,” *J. Acoust. Soc. Am.*, vol. 136, no. 1, pp. 242–247, 2014.
- [27] J. L. Cieřliński and B. Ratkiewicz, “On simulations of the classical harmonic oscillator equation by difference equations,” *Advances in Difference Equations*, vol. 2006, pp. 1–17, 2006.
- [28] J. Botts and L. Savioja, “Extension of a spectral time-stepping domain decomposition method for dispersive and dissipative wave propagation,” *J. Acoust. Soc. Am.*, vol. 137, no. 4, pp. EL267–EL273, 2015.
- [29] G. Strang, “The discrete cosine transform,” *SIAM Review*, vol. 41, no. 1, pp. 135–147, 1999.
- [30] C. F. Van Loan, *Computational Frameworks for the Fast Fourier Transform*, SIAM, 1992.
- [31] J. T. Etgen, “Accurate wave equation modeling,” *SEP-60: Stanford Exploration Project*, vol. 131, pp. 148, 1989.
- [32] F. B. Hildebrand, *Finite Difference Equations and Simulations*, Prentice-Hall, Englewood Cliffs, NJ, 1968.

- [33] W. F. Ames, *Numerical Methods for Partial Differential Equations*, Academic Press, 2nd edition, 1977.
- [34] B. Hamilton, S. Bilbao, and C. J. Webb, "Improved finite difference schemes for a 3-D viscothermal wave equation on a GPU," in *Proc. Forum Acusticum*, Krakow, Poland, Sept. 2014.
- [35] C. G. M. Desvages, *Physical modelling of the bowed string and applications to sound synthesis*, Ph.D. thesis, The University of Edinburgh, 2018.
- [36] C. Desvages and S. Bilbao, "Optimised passive discrete-time models of frequency-dependent loss in linear strings," in *Proc. Int. Conf. Sound & Vibration*, Montréal, Canada, July 2019.
- [37] M. Ducceschi and C. J. Webb, "Plate reverberation: Towards the development of a real-time physical model for the working musician," in *Proc. Int. Cong. Acoust.*, Buenos Aires, Argentina, 2016.
- [38] J. Antoni, "Orthogonal-like fractional-octave-band filters," *J. Acoust. Soc. Am.*, vol. 127, no. 2, pp. 884–895, 2010.
- [39] J. B. Allen and D. A. Berkley, "Image method for efficiently simulating small-room acoustics," *J. Acoust. Soc. Am.*, vol. 65, pp. 943, 1979.
- [40] E. De Sena, N. Antonello, M. Moonen, and T. van Waterschoot, "On the modeling of rectangular geometries in room acoustic simulations," *IEEE/ACM Trans. Audio, Speech, Lang. Process.*, vol. 23, no. 4, pp. 774–786, 2015.
- [41] A. Southern, S. Siltanen, D. Murphy, and L. Savioja, "Room impulse response synthesis and validation using a hybrid acoustic model," *IEEE Trans. Audio, Speech, Lang. Process.*, vol. 21, no. 9, Sept. 2013.
- [42] D. Fogerty, A. Alghamdi, and W.-Y. Chan, "The effect of simulated room acoustic parameters on the intelligibility and perceived reverberation of monosyllabic words and sentences," *J. Acoust. Soc. Am.*, vol. 147, no. 5, pp. EL396–EL402, 2020.
- [43] P. A. Naylor and N. D. Gaubitch, *Speech Dereverberation*, Springer Science & Business Media, 2010.
- [44] B. Hamilton, C. J. Webb, N. D. Fletcher, and S. Bilbao, "Finite difference room acoustics simulation with general impedance boundaries and viscothermal losses in air: Parallel implementation on multiple GPUs," in *Proc. Int. Symp. Music & Room Acoust.*, Buenos Aires, Argentina, Sept. 2016.
- [45] H. Lai and B. Hamilton, "Computer modeling of barrel-vaulted sanctuary exhibiting flutter echo with comparison to measurements," *Acoustics*, vol. 2, no. 1, pp. 87–109, 2020.
- [46] S. Bilbao and B. Hamilton, "Directional sources in wave-based acoustic simulation," *IEEE/ACM Trans. Audio, Speech, Lang. Process.*, vol. 27, no. 2, pp. 415–428, 2018.
- [47] S. Bilbao, A. Politis, and B. Hamilton, "Local time-domain spherical harmonic spatial encoding for wave-based acoustic simulation," *IEEE Signal Process. Lett.*, vol. 26, no. 4, pp. 617–621, 2019.